

# Can galactic nuclei be non-axisymmetric? — The parameter space of power-law discs

HongSheng Zhao, C. Marcella Carollo & P. Tim de Zeeuw <sup>★</sup>

*Sterrewacht Leiden, Niels Bohrweg 2, 2333 CA, Leiden, The Netherlands*  
*Johns Hopkins University, 3701 San Martin Drive, Baltimore MD 21218, USA*

Accepted ... Received ...; in original form ...

## ABSTRACT

The shape of a cusped galactic nucleus is constrained by the range of shapes of orbits in its gravitational potential. It is shown for scale-free non-axisymmetric discs that while a plausible elongated density model requires at least some orbits to spend more time near the major axis than anywhere else, both regular boxlets and tube orbits generally cross the major axis too fast for self-consistency. If galaxies host inner nuclear discs or flat bars with a cuspy surface light profile ( $\gamma = |d \log \mu / d \log r| > 0$ ), their ellipticity  $1 - b/a$  cannot be greater than about  $\gamma/2$ . Discs or bars with a shallow central profile ( $\gamma \leq 0.3$ ) should not be strongly elliptical.

**Key words:** galaxies: kinematics and dynamics

## 1 INTRODUCTION

Current formation theories emphasize the roles of dissipation and galaxy interaction as major processes in shaping present day galaxies, but is there any stringent limit on the shapes and density profiles of galaxies from general conditions such as equilibrium and stability alone? Particularly, are there stable triaxial equilibria with realistic radial density profiles? This has been an out-standing stellar dynamical question ever since Binney (1978) invoked triaxial equilibria to account for the observed flattened shape of elliptical galaxies and their lack of rotation. Theoretically triaxial equilibria exist at least for systems with a finite density core and a wealth of box orbits and tube orbits. This was demonstrated for general models by Schwarzschild (1979, 1982), and for models with separable potentials by Statler (1987). However, the traditional assumption of a finite core in every galaxy was challenged by recent observations of nuclei of nearby elliptical galaxies with the Hubble Space Telescope. It was found that giant ellipticals have a power-law surface density distribution  $\mu \propto r^{-\gamma}$  with  $0 < \gamma < 0.3$  near the center; the slope steepens to as much as 0.3–1.3 for small ellipticals, with the dividing line at  $M_B \approx -20$  mag (Crane et al. 1993; Jaffe et al. 1994; Lauer et al. 1995; Carollo et al. 1997; Faber et al. 1997). These observations call for a re-examination of the existence of triaxial equilibria in a potential with a divergent force ( $F \propto \mu \rightarrow \infty$  for  $\gamma > 0$ ) at the center (Gerhard & Binney 1985; de Zeeuw & Carollo 1996). Whether triaxial models of this kind exist also be-

comes a key uncertainty in, e.g., interpreting the kinematic and photometric data of galactic nuclei, weighing their central black holes and reconstructing the formation history of these systems.

The conclusion that at least some strongly non-axisymmetric models with a steep central cusp are probably not in rigorous steady state is based on a handful of three-dimensional dynamical models. These have been built with various implementations of Schwarzschild’s method, in which individual orbits are populated so as to match the model density, and include three-dimensional scale-free models with logarithmic potentials (Schwarzschild 1993), and two non-scale-free models (Merritt & Fridman 1996). Unfortunately, the power of these few numerical experiments is limited when it comes to exploring the parameter space. It is not clear how to extrapolate results obtained for a few models to a general statement about the whole class of cusped triaxial potentials, because the meaning of a small mismatch in the reconstructed density, which is often of the order of one percent or less, has to be interpreted on a case-by-case basis. Kuijken (1993, hereafter K93) showed in his systematic study of two-dimensional non-axisymmetric models with a logarithmic potential that whether the numerically constructed model is in equilibrium depends sensitively on numerical details, including the resolution of the spatial grid for the mass model, the grid for orbital initial conditions, the number of orbits used, and the integration time for each orbit. Although it may be feasible with present-day computer technology to carry out a massive numerical search in the multi-dimensional parameter space (axis ratios, inner and outer density slopes with the possible addition of a central black hole and the tumbling speed of the poten-

<sup>★</sup> E-mail: hsz@strw.leidenuniv.nl, marci@pha.jhu.edu, tim@strw.leidenuniv.nl

tial), it is intrinsically difficult in this approach to pinpoint the exact origin of any mismatch between the orbits and the density model. For example it has not been well-understood why replacing box orbits in a cored potential by boxlets in a cusped potential upsets the equilibria.

In this paper we present a new approach to study self-consistency of a general non-axisymmetric model. We restrict ourselves to the two-dimensional case of scale-free discs, and show that a non-trivial and necessary condition for the existence of a self-consistent elongated disc is that the angular speed of the regular boxlet and tube orbits when they cross the major axis should be consistent with the local curvature of the density distribution. It is well known that boxlets are less useful than box orbits when it comes to fit the model density near the major axis because the boxlets have their density maxima at the turning points rather than on the major axis (e.g., Pfenniger & de Zeeuw 1989; Schwarzschild 1993). K93 made the interesting observation that a box orbit has only one ‘corner’ per quadrant, while a boxlet orbit has two or more correlated ‘corners’ per quadrant, which makes them less flexible in fitting the model density. He also suggested that the lack of self-consistency in elliptical models is likely due to the spiky angular distribution of boxlets rather than to the lack of flattened boxlets. Syer & Zhao (1998, hereafter SZ98) suggested that the self-consistency is first broken down near the symmetry axes of the model. Unfortunately, the result of SZ98 is limited to a special subset of the separable non-axisymmetric potentials introduced by Sridhar & Touma (1997, hereafter ST97).

The structure of this paper is as follows. §2 gives a rigorous formulation of the problem for scale-free discs. §3 illustrates the requirement on the curvature of the model with specific orbits in elliptic disc potentials. §4 gives the results of fitting the curvature, and §5 examines the assumptions in the model, and discusses generalizations of the method to three-dimensional and non-scale-free systems, as well as the implications for barred galaxies.

## 2 SCALE-FREE NON-AXISYMMETRIC DISCS

### 2.1 Formulation

Consider a general two-dimensional scale-free non-axisymmetric disc potential

$$\phi(r, \theta) \propto r^\alpha p(\theta), \quad -1 \leq \alpha \leq 1, \quad (1)$$

where  $p(\theta)$  defines the angular shape, with  $\theta = 0$  and  $\pi/2$  the directions of the minor and major axis, respectively. We consider surface densities of the form

$$\mu(r, \theta) \propto r^{-\gamma} s(\theta), \quad 0 \leq \gamma < 2, \quad (2)$$

where  $\gamma$  is the cusp strength and  $s(\theta)$  the angular shape of the surface density. In self-consistent systems  $s(\theta)$  and  $p(\theta)$  are related, and  $\gamma = 1 - \alpha$ .

The regular orbits in this potential can be grouped according to their shapes (bananas, fishes, tubes, etc.; see Miralda–Escudé & Schwarzschild 1989; K93), irrespective of their sizes, into self-similar families. Each family can be characterized by a dimensionless second integral, say,  $I$ , and the whole family can be then built by rescaling one reference orbit with a trajectory described by the polar coordinates

$(r_I(t), \theta_I(t))$ . The weights among the self-similar ‘cousin’ orbits should be prescribed in a scale-free fashion such that each family produces a  $r^{\alpha-1}$  power-law density distribution, as for the model density. The different families should be weighed according to a to-be-determined positive function  $w(I) \geq 0$  so as to reproduce the angular part of the model density.

A clear discussion of the algorithm for constructing self-similar non-axisymmetric models was given by Richstone (1980) and Schwarzschild (1993) for three-dimensional models, and by K93 for two-dimensional models. These previous studies were focused exclusively on the logarithmic potential, and it appears that no one has applied the algorithm to other non-axisymmetric power-law potentials, which are most relevant for galactic nuclei. Following K93, we first divide the angular coordinate into  $n$  slices with an interval  $\Delta\theta = 2\pi/n$ , and  $n$  approaching infinity. We then compare the amount of mass a reference orbit deposits in each angular sector to the amount of mass required by the density model in the same sector within the radius of the orbit. If a reference orbit  $(r_I(t), \theta_I(t))$  spends a fraction  $\Delta(t/T)_{I,j}$  of the integration time  $T$  in the  $j$ -th sector, then it deposits an amount proportional to  $w(I)\Delta(t/T)_{I,j}$ . By comparison, the amount of mass prescribed by the density model in the same angular sector within the radius  $r_I(t)$  is,

$$\Delta m_{I,j} \equiv \Delta\theta \int_0^{r_I(t)} \mu(r_1, \theta) r_1 dr_1 \quad (3)$$

$$\propto r_I^2(t) \mu(r_I(t), \theta) \Delta\theta. \quad (4)$$

To reproduce the model density using regular orbits alone we require that

$$\int dI w(I) \left\langle \frac{\Delta(t/T)_{I,j}}{\Delta m_{I,j}} \right\rangle = 1, \quad j = 1, \dots, n \quad (5)$$

where we have taken time averages (as indicated by the brackets) of all the times when an orbit comes to the same angle, and have summed up all regular families by integrating the second integral  $I$ .

It is straightforward to verify this result for the scale-free logarithmic disc of K93. In this special case  $\mu \propto r^{-1} s(\theta)$ , so  $\Delta m_{I,j} \propto r_I(t) s(\theta) \Delta\theta$ . Eq. (5) can then be rewritten in a form similar to K93,  $\int dI w(I) \langle \Delta(t/T)_{I,j} / r_I(t) \rangle \propto s(\theta) \Delta\theta$ .

### 2.2 Curvature at the major axis

For the time being we assume that the angular momentum of a regular orbit is always non-zero everywhere in the orbit (which is clearly not the case near the turning point of a boxlet orbit), so that  $\dot{\theta}_I \neq 0$ . Taking the limit  $\Delta\theta \rightarrow 0$ , we have

$$\frac{\Delta t}{\Delta\theta} \rightarrow \|\dot{\theta}_I(t)\|^{-1}, \quad (6)$$

and upon substitution in eq. (5) and (3), we obtain

$$\int dI w(I) \langle \Gamma \rangle = \text{const}, \quad \Gamma \equiv \frac{1}{\mu(r, \theta) \|J\|}, \quad (7)$$

where the weights  $w(I)$  are non-negative and  $J \equiv r^2 \dot{\theta}$  is the angular momentum.

To examine how the orbits fit the curvature of the density near the major axis, we take the double derivative of

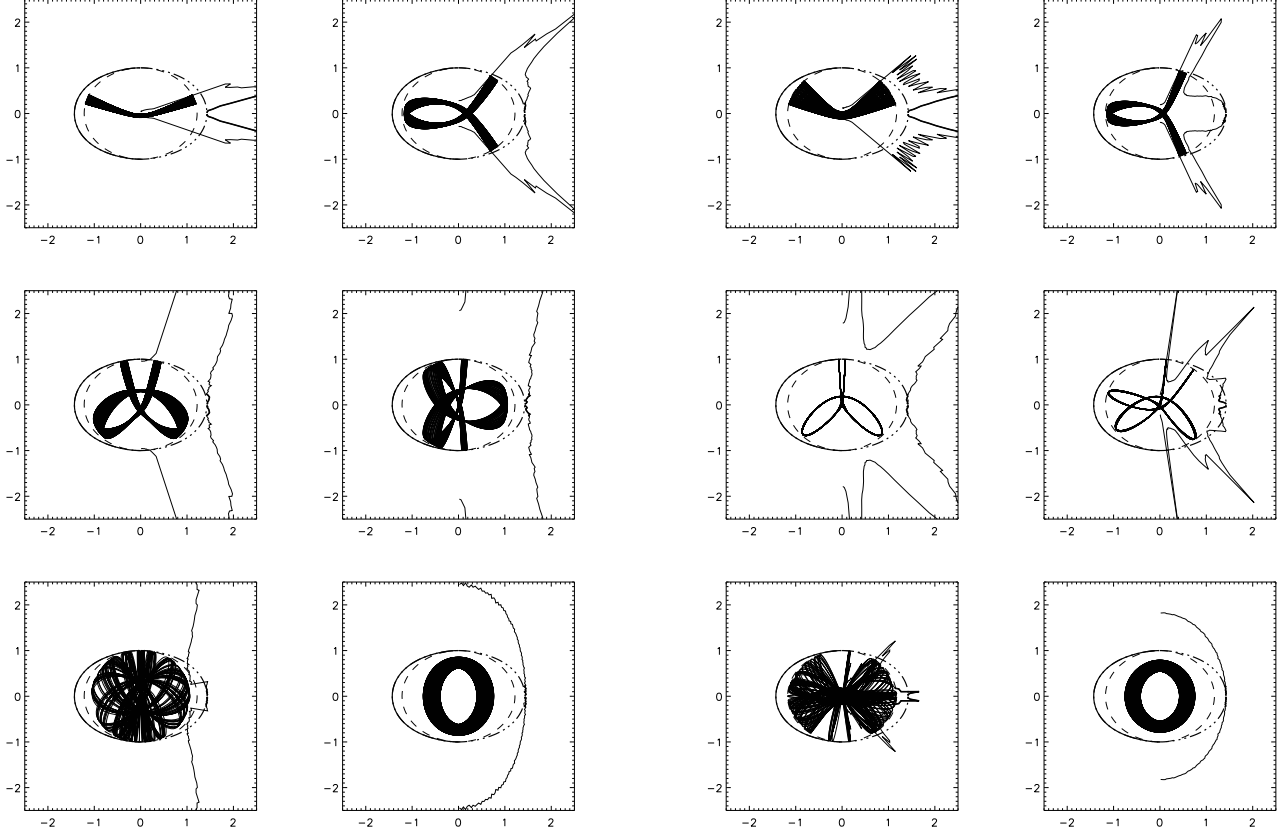


**Figure 1.** Various reference orbits (thin solid lines) with the same energy in a two-dimensional scale-free elliptic disc with a surface density power-law slope  $\gamma = 1 - \alpha = 0.8$  and axis ratio  $q = 0.7$ . The orbits shown are a regular banana orbit, a fish orbit, two high resonance orbits, a stochastic orbit and a tube orbit. Compare the shape of the orbits with the shapes of the overplotted zero-velocity curve (thin dashed line), the model density contour (dash-dotted line) and the contour made by summing up the spatial distribution of the ‘cousin’ orbits, the scaled and reflected copy orbits (the outer solid lines). Near the major axis the contours of these orbits bend in the opposite direction of the elliptical contours of the model density. The similar contours for tubes bend in the right direction, but not strong enough.

eq. (7) with respect to  $\theta$ , and substitute the result in the equations of motion

$$\ddot{r} = \frac{J^2}{r^3} - \frac{\partial\phi}{\partial r}, \quad \dot{\theta} = -\frac{\partial\phi}{\partial\theta}. \quad (8)$$

The angular momentum  $J$  is nearly constant in the vicinity of the major axis where the torque  $-\partial\phi/\partial\theta \rightarrow 0$ , because the force is radial at the symmetry axes. Evaluating the angular derivatives at the major axis of the potential ( $\theta = \pi/2$ ), we obtain the following simple expression (see Appendix A for a derivation):

$$\int dI w(I) \left\langle [q_\phi^{-2} - (1 + \gamma - \gamma\lambda)] \frac{\Gamma}{K_\theta} \right\rangle = 0, \quad (9)$$

where

$$\lambda \equiv (1 + \gamma)K_r + q_\mu^{-2}K_\theta|_{\theta=\pi/2} > 0, \quad (10)$$

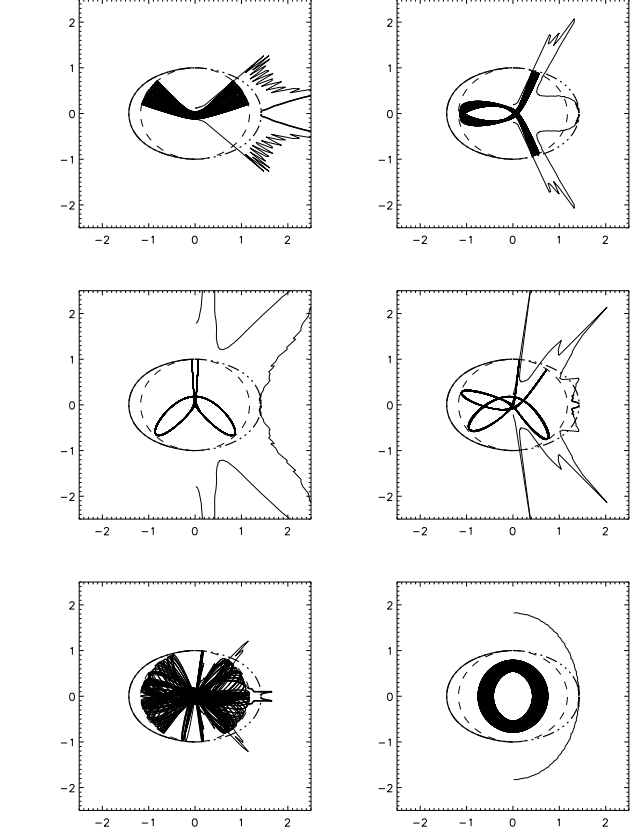


**Figure 2.** As Figure 1, but for an elliptic disc with a surface density power-law slope  $\gamma = 1 - \alpha = 1.2$  and axis ratio  $q = 0.7$ . Only the fish orbit supports the potential near the major axis.

and we have written  $K_r \equiv \frac{\dot{r}^2}{r\partial_r\phi}$  and  $K_\theta \equiv \frac{r^2\dot{\theta}^2}{r\partial_r\phi}$  as the radial and tangential parts of the kinetic energy scaled by the virial  $r\partial_r\phi$ . The quantities  $q_\phi^{-2}$  and  $q_\mu^{-2}$ , defined as

$$q_X^{-2} \equiv 1 + \frac{\partial_\theta^2 X}{r\partial_r X}|_{\theta=\pi/2}, \quad X = [\phi(r, \theta), \mu(r, \theta)] \quad (11)$$

describe the curvatures of the equal potential and equal density contours at the major axis (alternative expressions in terms of double derivatives of  $s(\theta)$  and  $p(\theta)$  are given by eqs A6 and A7). Here  $q_{[\phi, \mu]}$  are the axis ratios of the best-fitting ellipses to the potential, respectively density, contours near the major axis. A similar result can be derived for any angle  $\theta$ , but the expression is much simpler at the symmetry axes because all first derivatives vanish:  $\partial_\theta\mu(r, \theta) = \partial_\theta\phi(r, \theta) = \partial_\theta J = 0$ ; the result on the minor axis turns out to be not very useful in providing constraints to models. We remark that, e.g., circular orbits in an axisymmetric system trivially satisfy eq. (9) because  $q_\mu = q_\phi = \lambda = 1$ .

### 3 ORBITS IN ELONGATED DISCS

Consider scale-free discs with surface density of the form:

$$\mu(r, \theta) \propto r^{-\gamma} (\cos^n \theta + q^n \sin^n \theta)^{-\frac{\gamma}{n}}. \quad (12)$$

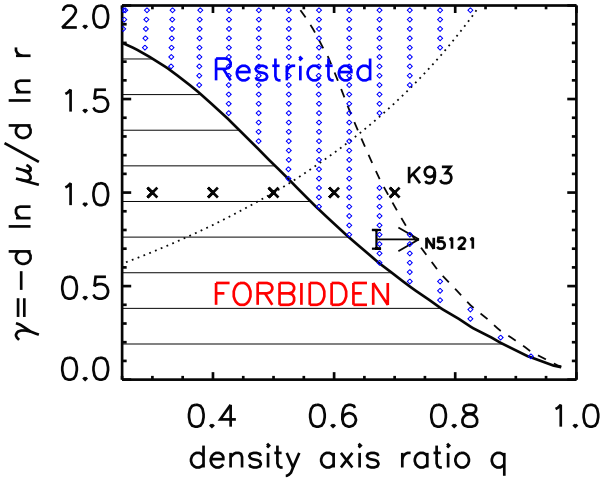


**Figure 3.** The parameter space for scale-free discs: cusp-slope  $\gamma$  versus axis ratio  $q$ . No self-consistent elliptic discs can occupy the shaded region to the left of the solid line (where  $1 - q > \gamma/2$ ), due to the wrong curvature of orbits at the major axis. Regions to the left of the dashed curve ( $h < 0.5$ , see §5.2) and/or the dotted line ( $C < 0.707$ , see §5.3) are also restricted by the shapes of the available orbits. The crosses indicate logarithmic elliptic discs which are found to be likely non-self-consistent in previous numerical studies by Kuijken (1993). The error bar indicates the cusp strength for the nuclear bar in NGC5121 observed by HST.

The gravitational potential of these discs is not exactly elliptical, and is formally given by eq. (1). It can be computed with harmonic expansions as in SZ98. When  $n = 2$ , the surface density is stratified on ellipses of axis ratio  $q$ .

Figures 1 and 2 show the density distribution of the dominant orbits in two such discs. The heavy solid line in each panel indicates the shape of the orbit after all the scaled copy orbits and their reflection images are summed up in a scale-free fashion; for clarity only the right hand part is drawn. We find that near the major axis the density contributions of all tube orbits, and nearly all boxlet orbits, curve in the opposite sense as the model density; the exceptions are the fish orbits in some potentials (Miralda-Escudé & Schwarzschild 1989; K93), which sometimes support the curvature of the model density.

The above result suggests that a large fraction of scale-free elliptic disc potentials cannot be made self-consistent near the major axis. While the tube orbits are always anti-aligned with the potential (e.g., de Zeeuw, Hunter & Schwarzschild 1987), once the ‘backbone’ of a cored potential, namely the set of box orbits, is replaced by the boxlets and stochastic orbits of a cusped model, there may be no orbits left to support the potential near the major axis. Since a general property of all orbits is that the amplitude of the orbital angular momentum always reaches a local maximum on the major axis, an orbit tends to spend more time away from the major axis than on the axis. As a result, the curvature of orbits is often opposite to the real density even after all ‘cousin’ orbits are added, which limits the range of non-axisymmetric models with cusps that can be self-consistent.

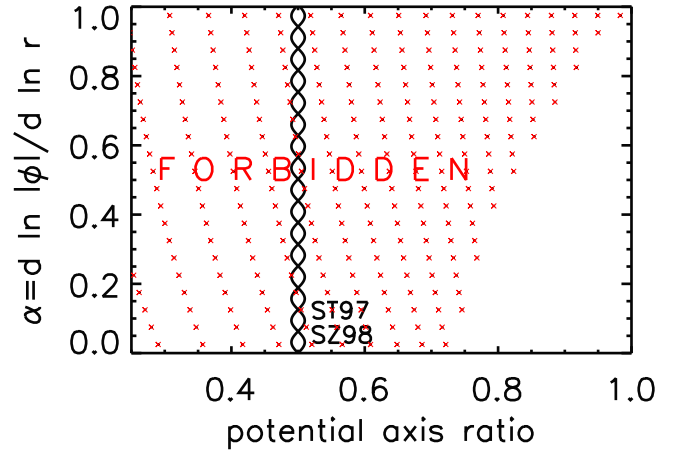


**Figure 4.** The parameter space of non-axisymmetric disc potentials. Self-consistency is ruled out for a large fraction of discs with elliptical density contours (indicated by small crosses) and for the whole sequence of cuspy, separable potentials of axis ratio 0.5 studied by Sridhar & Touma (1997) and Syer & Zhao (1998) (figure-eight symbols). The axis ratio here is for the equal potential contours, although they are generally not exactly elliptical.

#### 4 FITTING THE CURVATURE AT THE MAJOR AXIS

We now present a more quantitative analysis of the curvature of the regular orbits. A simple and necessary condition for self-consistency near the major axis of the model follows from eq. (9): at least some orbits should have a negative  $[q_\phi^{-2} - (1 + \gamma - \gamma\lambda)]$  and others a positive value in order to place the average at zero. This places a range on the possible curvature (or axis ratio) of the potential, as follows:

$$[0, 1 + \gamma - \gamma\lambda_{\max}]_{\max} \leq q_\phi^{-2} \leq [1, 1 + \gamma - \gamma\lambda_{\min}]_{\min}. \quad (13)$$

Since  $\infty > \lambda_{\max} \geq \lambda \geq \lambda_{\min} > 0$  by definition (cf eq. (10)), a clean non-trivial limit is that

$$q_\phi > \frac{1}{\sqrt{1 + \gamma}}. \quad (14)$$

This condition turns out to be quite powerful. It implies that discs with shallow density cusps (small  $\gamma$ ) cannot have a highly elliptical potential because they would violate the requirement of the curvature. The curvature condition is trivially satisfied in the Keplerian regime, since the potential becomes spherical ( $q_\phi^{-2} \rightarrow 1$ ). This would be the case near a central black hole, or at very large distance of a model with a finite mass.

Our analysis nicely confirms the result of the semi-analytical study of SZ98 that all ST97 discs are non-self-consistent. Eq. (14) is always violated for these discs, because

$$q_\phi = \frac{1}{\sqrt{3 - \gamma}} < \frac{1}{\sqrt{1 + \gamma}} \quad \text{for ST97 discs with } \gamma < 1; \quad (15)$$

ST97 models with  $1 < \gamma < 2$  have unphysical negative density regions.

More interesting is the application of the curvature criterion (14) to the entire class of elongated discs. Self-

consistent elliptic discs ( $n = 2$  in eq. (12)) must have strong enough cusps such that

$$\gamma > q_\phi^{-2} - 1 \approx 2(1 - q_\mu), \quad (16)$$

where  $q_\mu = q$  is the axis ratio of the surface density.

Figure 3 shows that about 50% of the parameter space in the cusp strength vs axis-ratio plane of elliptic discs can be simply ruled out on the basis of examining the curvature at the major axis. Figure 4 shows a similar diagram, but for the potential of elliptic discs and the ST97 models. When applied to the specific case of the  $\gamma = 1$  elliptic disk, the lower limit on the allowed axis ratio provided by eq. (14) is in harmony with the numerical estimates of K93.

Perhaps unexpectedly, our criterion shows that non-axisymmetric discs with a shallow cusp are easier to rule out than those with strong cusps, while the opposite has been suggested for three-dimensional models, based on numerical experiments with two classes of potentials, one with a finite force at the center ( $\gamma = 0$  in projection), the other with the force diverge as  $r^{-1}$  ( $\gamma = 1$ ) (Merritt & Fridman 1996). These two opposing suggestions here may well reflect the still incomplete coverage of parameter spaces of both approaches: we are restricted to 2D scale-free discs, but we gain better coverage of the range of cusp slope  $\gamma$  and ellipticity  $1 - q$  owing to our analytical approach.

## 5 DISCUSSION AND CONCLUSIONS

We have shown that many scale-free elliptic discs cannot be self-consistent, and we have given specific criteria for picking out non-self-consistent models. The major axis is a local maximum in terms of the angular momentum of an orbit, which often translates to a local minimum in terms of the fraction of time spent by regular boxlets and tube orbits. This is opposite to that required by the surface density distribution. A clean result from this analysis is shown by the forbidden zone in Fig. 3, which implies that galactic nuclear discs with a shallow density profile ( $0 \leq \gamma \leq 0.3$ ) are necessarily nearly axisymmetric.

### 5.1 Hidden assumptions

Our results apply only to orbits which cross the disc major axis with a finite angular momentum  $\|J\| \equiv r^2 \|\dot{\theta}\|$ , so that  $\|\dot{\theta}\|^{-1}$  and its derivatives are well-defined at  $\theta = \pi/2$ . This condition clearly breaks down for the axial orbits and/or the stochastic orbits. The two are perhaps the same since the axial orbits are destabilized by the divergent force at the center, and become stochastic.

Stochastic orbits make our method problematic because they could reach  $J = 0$  virtually anywhere. And it is quite inevitable that they will be populated during galaxy formation. However, the way they are populated must be restricted in an equilibrium model because stochastic orbits are slowly-evolving orbits. The only sure recipe to mix stochastic orbits of the same energy ( $E_0$ ) together into a time-independent building block (a super-orbit) is with a distribution function  $\delta(E - E_0)$  (Zhao 1996); this distribution mixes in the regular orbits of the same energy  $E_0$  as a side effect. In our scale-free models these super-orbits form one family, with the relative weights of all members

related by a simple scaling (§2). Fortunately for the present problem, the spatial distribution of this super-orbit family is always as round as the equal-potential contours. Since the equal-density contours are generally more elongated, including the super-orbits does not relax our constraints on curvature.<sup>†</sup> So in summary, our result remains valid if stochastic and/or axial orbits are populated with a time-independent distribution.

Can a small operation near the major axis of the density model bring the model to self-consistency? One possibility is to modify the shape of the equal-density contour near the major axis by a significant amount (without violating the Poisson equation and the positivity of the density) such that it is rounder than that of the equal potential contour ( $q_\mu > q_\phi$ ) *locally*. It is conceivable that by heavily populating the super-orbit component, which is stratified on a set of mildly elongated equal-potential contours, one might counteract the wrong curvature from regular orbits at the major axis. Whether self-consistency can be restored this way also depends on the maximum fraction of mass which can be allocated to the super-orbit component.

### 5.2 Expanding the forbidden territory

Can self-consistent scale-free discs be ruled out on the right-hand side of the ‘forbidden zone’ in Figure 3? Perhaps this is likely: if regular orbits always have a finite (rescaled) angular momentum  $h$  when crossing the major axis, and orbits with less angular momentum are stochastic, then the minimum angular momentum sets up a barrier to prevent any regular orbit from falling to the center or touching the zero-velocity curve on the major axis. Here  $h$  is defined by  $0 < h \equiv J_{\min}^2/J_E^2 \leq 1$ , where  $J_E$  is the maximum angular momentum allowed for an orbit of energy  $E$ . There should be a gap in phase space filled by stochastic orbits which separates the unstable periodic axial orbit from the regular boxlets. Such a stochastic gap is typically seen in the start space on the zero-velocity surface of three-dimensional models, and in surfaces of section along the major axis of two-dimensional models (e.g., fig. 5 of Schwarzschild 1993). The minimum angular momentum sets up a dynamical boundary to  $r$ ,  $r\partial_r\phi$ ,  $\dot{r}$  and  $\lambda$  (cf eq. (10)) at the upper and lower ends. The upper limit on  $\lambda$  typically helps little to tighten the constraints, but the finite lower limit of  $\lambda$ , namely  $\lambda_{\min}(h)$  as a function of  $h$ , propagates to a more stringent upper limit on the flattening (cf eq. (13)) and pushes the limit of the forbidden region further to the right in Figure 3. The parameter space to the left of the dashed line can be ruled out as long as the stochastic gap is wide enough ( $h > 0.5$ ). Typically only fish orbits or higher-order resonant orbits can have a small  $h$ , and we suspect that it is difficult to reach self-consistency for much of the region to the right of the forbidden zone

<sup>†</sup> It is possible to modify the shape of a super-orbit by subtracting the densities of regular orbits from it—always keeping the density everywhere non-negative. It is not clear whether the resulting component (a nearly spherical distribution with many wormholes) will be more elongated than the density model. Even if it were to do so, we suspect that it would not relax the constraint on the intrinsic shape of the model unless this single component is also very heavily populated during galaxy formation.

in Fig. 3 without heavily populating the higher-order resonances. This hypothesis is also supported by the range of non-self-consistent models of K93 (indicated by the crosses), which extends to our  $h = 0.5$  line.

### 5.3 Constraint from the density contrast

The density ratio of the minor vs. major axis should also set limits on the ellipticity of self-consistent discs. As shown by SZ98, if

$$C \equiv \left[ \frac{\mu(r, 0)}{\mu(r, \frac{\pi}{2})} \right] \left[ \frac{\phi(r, 0)}{\phi(r, \frac{\pi}{2})} \right]^{\frac{\gamma}{\alpha}} \equiv \left( \frac{1 - \epsilon_\mu}{1 - \epsilon_\phi} \right)^\gamma, \quad (17)$$

is defined as a measure for the model density contrast between the minor and major axes, where  $1 - \epsilon_\mu$  and  $1 - \epsilon_\phi$  are the minor-to-major axis ratio of the equal density and equal potential contours respectively, then  $C$  must have a non-trivial lower and upper bound,

$$C_{min} \leq C \leq C_{max}, \quad (18)$$

set by the shape of orbits in the potential. A model constructed by populating only the thinnest banana orbit in a potential cannot be flatter than a certain value because of the fact that even the thinnest banana orbits spend a fair amount of time near the minor axis. Populating thick boxlet orbits, higher-order resonant orbits and tube orbits tend to make the shape rounder as these orbits come more frequently to the minor axis than the thin banana orbits. Figure 3 also shows the curve with  $C = 0.707 \approx 1/\sqrt{2}$  in the  $q$  vs.  $\gamma$  plane. This curve is interesting for reference as it corresponds to a configuration where only the thinnest banana orbits in a ST97 potential are populated. In contrast a  $C = 1$  curve (which means  $\epsilon_\mu = \epsilon_\phi$ ) would correspond to a configuration where only the  $f(E)$  super-orbits are populated. The realistic configurations are likely in between these extremes. Combined with the criteria from the curvature, Figure 3 suggests that about 2/3 of the parameter space of cusped elliptic discs are ruled out.

### 5.4 Implications for nuclear discs and bars

Our curvature constraint on the existence of self-consistent scale-free elliptic disks can be applied to the properties of observed stellar bars and nuclear discs. The dynamics of these highly flattened systems are essentially two-dimensional with the small vertical oscillation completely decoupled from the motion in the plane. In the absence of a curvature criterion for three-dimensional models, it is premature to discuss the parameter space for elliptical galaxies.

Tumbling stellar bars have scales set by the corotation radius. Numerical experiments show that regular boxlet or loop orbits have a central ‘hole’ of finite size compared to their apocenter. So one expects a region infinitely close to the center where no ‘large’ orbits will ever visit. The dynamics of the very nucleus will be dominated by ‘small’ orbits *in situ*. Such a situation would not be possible for models with a finite core. We know of at least one set of strongly elongated bar models — the rotating Freeman (1966) elliptic discs, which can be built self-consistently for any axis ratio. Our curvature condition clearly does not apply to these models with an analytical core ( $\gamma = 0$ ) as the finite force at

the center stabilises axial orbits and box orbits. But it can be applied with confidence to the central regions of cusped elliptical nuclear bars. And our results show that these cannot be strongly elongated; their axis ratio in projected light should satisfy the major axis curvature condition eq. (14).

Our curvature constraint on elongation comes from the general property that the orbital angular momentum peaks near the major axis, so that the orbital density generally has a local minimum on this axis, whereas the model density is largest there. We therefore expect it to hold to some extent for general discs, as long as a genuine cusp ( $\gamma \neq 0$ ) in the central surface density creates a divergent force at the center and destabilises any box orbit. An outer truncation of the mass distribution and the tumbling motion of the bar can greatly change the potential at large radius, but at very small radii the model reduces to the static self-gravitating scale-free case. This happens at radii well-inside the ILR of any rotating potential (but well beyond the sphere of influence of any small central black hole if it exists in bars) such that the centrifugal and Coriolis forces are negligible compared to the self-gravity of the cusp.

Measurements of nuclear cusp slopes for galaxies with nuclear bars are as yet scarce. The one object for which the light distribution has been measured with HST resolution, NGC 5121, shows a steep light profile with  $\gamma = (0.75 \pm 0.05)$  and a projected axis ratio  $(0.67 \pm 0.05)$  (Carollo & Stiavelli 1998). This data point, as shown in Fig. 3, is safely outside the forbidden zone with or without correcting for the inclination. Imaging of other nuclear bars are needed to establish whether there is a zone of avoidance for the shapes of cusped galaxies.

It is a pleasure to acknowledge helpful discussions with Vincent Icke, Konrad Kuijken, Doug Richstone, Massimo Stiavelli, Scott Tremaine, and Dave Syer, and thoughtful suggestions by an anonymous referee which helped to improve the presentation of our results.

## APPENDIX A: DERIVATION FOR DOUBLE DERIVATIVE OF $\Gamma$

The lengthy calculation of the double derivative of  $\Gamma$  with respect to  $\theta$  is greatly simplified near the major axis ( $\theta = \frac{\pi}{2}$ ), where we can safely ignore any first or third derivatives of an even function with respect to time  $t$  or angle  $\theta$ , since these tend to zero.

First we decompose the double derivative of  $\Gamma$  (cf. eq. 7) at  $\theta = \frac{\pi}{2}$  to that with respect to radius  $r$ , to angular momentum  $J$ , and to the angular part  $s(\theta)$  of the density,

$$\frac{d^2\Gamma}{\Gamma d\theta^2} \Big|_{\theta=\frac{\pi}{2}} = -\frac{d^2J}{Jd\theta^2} + \frac{d^2r^\gamma}{r^\gamma d\theta^2} - \frac{d^2s(\theta)}{sd\theta^2}. \quad (A1)$$

With the help of the equations of motion (eq. 8) we find

$$\frac{d^2J}{Jd\theta^2} = \frac{dJ}{J\dot{\theta}d\theta} \quad (A2)$$

$$= -\frac{\partial_\theta^2 \phi}{r^2 \dot{\theta}^2} \quad (A3)$$

$$\frac{d^2r^\gamma}{r^\gamma d\theta^2} = \gamma \frac{\ddot{r}}{r\dot{\theta}^2} + \gamma(1+\gamma) \left( \frac{dr}{rd\theta} \right)^2 \quad (A4)$$

$$= \gamma \frac{\dot{\theta}^2 r - \partial_r \phi}{r\dot{\theta}^2} + \gamma(1+\gamma) \left( \frac{\dot{r}}{r\dot{\theta}} \right)^2. \quad (A5)$$

Now rewrite the second derivatives of the density  $\mu$  and the potential  $\phi$  in terms of the curvatures of the density and potential, which by definition (cf. eq. 11) satisfy

$$q_\mu^{-2} - 1 = \frac{\partial_\theta^2 \mu}{r \partial_r \mu} = \frac{\partial_\theta^2 s(\theta)}{s} \frac{1}{-\gamma}, \quad (\text{A6})$$

$$q_\phi^{-2} - 1 = \frac{\partial_\theta^2 \phi}{r \partial_r \phi} = \frac{\partial_\theta^2 p(\theta)}{p} \frac{1}{1 - \gamma}. \quad (\text{A7})$$

Rewriting  $\dot{r}^2$  and  $\dot{\theta}^2$  in terms of  $K_r$  and  $K_\theta$ , we obtain

$$\frac{d^2 \Gamma}{\Gamma d\theta^2} \Big|_{\theta=\frac{\pi}{2}} = K_\theta^{-1} [q_\phi^{-2} - (1 + \gamma)(1 - \gamma K_r) + \gamma q_\mu^{-2} K_\theta], \quad (\text{A8})$$

which immediately reduces to eq. (9).

## REFERENCES

- Binney J.J., 1978, MNRAS, 183, 501  
 Carollo C.M., Franx M., Illingworth G.D., Forbes D.A., 1997, ApJ, 481, 710  
 Carollo C.M., Stiavelli M., 1998, AJ, 116, 68  
 Crane P., et al., 1993, AJ, 106, 1371  
 de Zeeuw P.T., Carollo C.M., 1996. In IAU Symposium 171, *New Light on Galaxy Evolution*, eds R. Bender, R.L. Davies (Dordrecht: Kluwer), 47  
 de Zeeuw P.T., Hunter C., Schwarzschild M., 1987, ApJ, 317, 609  
 Faber S.M., et al., 1997, AJ, 114, 1771  
 Freeman K.C., 1966, MNRAS, 134, 15  
 Gerhard O.E., Binney J.J., 1985, MNRAS, 216, 467  
 Jaffe W., Ford H.C., O'Connell R.W., van den Bosch F.C., Ferrarese L., 1994, AJ, 108, 1567  
 Kuijken K., 1993, ApJ, 409, 68 (K93)  
 Lauer T.R., et al., 1995, AJ, 110, 2622  
 Merritt D.R., Fridman T., 1996, ApJ, 460, 136  
 Miralda-Escudé J., Schwarzschild M., 1989, ApJ, 339, 752  
 Pfenniger D., de Zeeuw P.T., 1989, in *Dynamics of Dense Stellar Systems*, Cambridge Univ. Press, 1989, 81  
 Richstone D.O., 1980, ApJ, 238, 103  
 Schwarzschild M., 1979, ApJ, 232, 236  
 Schwarzschild M., 1982, ApJ, 263, 599  
 Schwarzschild M., 1993, ApJ, 409, 563  
 Sridhar S., Touma J., 1997, MNRAS, 287, L1 (ST97)  
 Statler T.S., 1987, ApJ, 321, 113  
 Syer D., Zhao H.S., 1998, MNRAS, 296, 407 (SZ98)  
 Zhao H.S., 1996, MNRAS, 283, 149